Inorganic Chemistry

ARTICLE

pubs.acs.org/IC

# Length-Controllable Catalyzing-Synthesis and Length-Corresponding Properties of FeCo/Pt Nanorods

Ming Wen,* Xiangguo Meng, Baolei Sun, Qingsheng Wu,* and Xiaolan Chai

Department of Chemistry, Tongji University, Shanghai 200092, The People's Republic of China

**ABSTRACT:** Newly designed magnetic-alloy/noble-metal FeCo/Pt nanorods have been first reported and fabricated through a length-controllable catalyzing-synthesis process in which the growth of FeCo nanorods was induced on Pt nanotips. The length of FeCo/Pt nanorods depends on the number of platinum nanotips. The proposed synthesis mechanism was corroborated by scanning electron microscopy, transition electron microscopy, X-ray diffraction, energy dispersive X-ray spectroscopy, and X-ray photoelectron spectroscopy. With the decrease of Fe content in $Fe_xCo_{96-x}/Pt_4$ nanoalloys from 77 to 15, the morphology changes from nanorods with different lengths to nanoparticles. The analysis of the magnetic hysteresis loops indicated that the magnetic saturation and coercivity were strongly dependent on the length of the nanorods in which maximum saturation magnetization and minimum coercivity were obtained for $Fe_{77}Co_{19}/Pt_4$ nanorods with the length of ~2.5 $\mu$m. In particular, FeCo/Pt exhibited length-dependent reactivity towards 1,1,2,2-tetrachloroethane, and $Fe_{77}Co_{19}/Pt_4$ nanorods with the length of ~2.5 $\mu$m yielded the greatest dechlorination rate. Moreover, Pt can enhance the dechlorination of 1,1,2,2-tetrachloroethane.

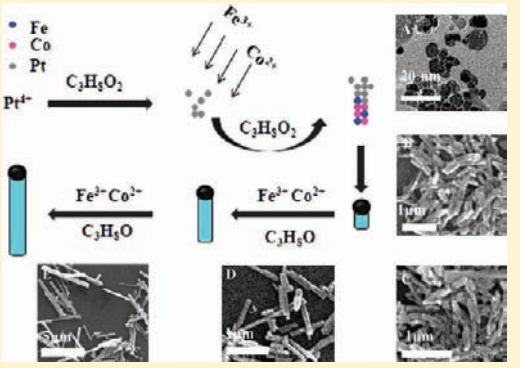


## 1. INTRODUCTION

One-dimensional (1D) magnetic nanostructures have attracted considerable attention owing to their distinctive properties and potential applications.[1] Especially, extensive theoretical and experimental efforts have been devoted to develop new 1D magnetic alloy nanostructures for their applications in magnetic information storage media, catalysis, environment treatment, biomedical, and so on. Because bimetallic alloys represent a viable route to tune the magnetic parameters that are strongly influenced by the compositional effect and lattice distortion, structurally distorted alloys like bct-FeCo[2] and FePt[3] may have high magnetic anisotropy energy values. Among the candidates of 1D magnetic alloy materials, FeCo alloy nanorods are the most outstanding soft-magnetic materials and have attracted great interest due to their unique magnetic properties, including the excellent magnetic anisotropy energy, large permeability, high saturation magnetization, low magnetostriction, high resistivity, low coercive force, and high Curie temperature, etc.[4−6] However, synthesis of the 1D FeCo magnetic nanorods by novel and facile solution chemical methods still remains a challenging task due to the difficult growth process of FeCo nanorods, although there are some reports on the synthesis of FeCo nanorods through template or electrochemical treatments.[7]

Platinum-included metallic heterostructure nanomaterials have been advancing since the resulting structures often have multifunctional capabilities with tunable and enhanced properties. The reported multimetallic nanomaterials, such as FePt, FeNiPt, and FeEuPt nanorods,[8,9] Pt@Pd core−shell particles,[10] Pt-on-NiCo[11] nanostructures, CoPt nanocrystals,[12] etc., often exhibit properties that are distinct from their constituent metals. However, to the best of our knowledge, few reports were concerned with the synthesis of magnetic-alloy/noble-metal FeCo/Pt nanorods. In this nanostructure, the advantage of FeCo alloy nanorods together with the function of Pt may introduce new multifunctional nanomaterials, which will bring potential applications to electronics, magnetism, environment remediation, and catalysis.

In this work, we first report new magnetic-alloy/noble-metal FeCo/Pt nanorods with well-controlled length through the catalyzing-synthesis process. On the basis of the inducing catalysis of Pt nanotips, an FeCo alloy can grow up to an FeCo/Pt nanorod in a template-absent chemical reaction system. The active catalysis characteristic of platinum joined with magnetic zerovalent FeCo nanorods substantially leads to a sufficient environmental remediation of a model chlorinated hydrocarbon. This effective approach offers much better control of both the length and the composition of FeCo/Pt nanoalloys. With the decrease of the Fe content in $Fe_xCo_{96-x}/Pt_4$ from 77 to 15, the morphology changes from nanorods to nanoparticles. In addition, the potential of the FeCo/Pt nanorods for environmental remediation of a model chlorinated hydrocarbon was performed in present work. 1D nanosized effects of FeCo magnetic nanorods, together with the intrinsic characteristic of the active site of Pt, substantially result in the length-controllable properties on the magnetic behavior and the dechlorination of 1,1,2,2-tetrachloroethane.

**Received:** May 12, 2011
**Published:** September 08, 2011

**Table 1. Molar Ratio of Metal Ions in Initial Solution and the Component of FeCo/Pt Nanoalloys with Their Magnetization ($M_s$) and Coercivity ($H_c$)**

| sample no. | initial molar ratios of Fe:Co:Pt | alloy content (%) | length ($\mu$m) | $H_c$ (Oe) | $M_s$ (emu/g) |
|---|---|---|---|---|---|
| S0 (nanorods) | 90:10:4 | $Fe_{82}Co_{14}/Pt_4$ | 4 | | |
| S1 (nanorods) | 80:16:4 | $Fe_{77}Co_{19}/Pt_4$ | 2.5 | 240 | 187 |
| S2 (nanorods) | 72:24:4 | $Fe_{69}Co_{27}/Pt_4$ | 2 | 256 | 172 |
| S3a (nanorods) | 48:48:4 | $Fe_{40}Co_{56}/Pt_4$ | 1.7 | 430 | 163 |
| S3b (nanoparticles) | 48:48:4 | $Fe_{40}Co_{56}/Pt_4$ | | 401 | 148 |
| S4 (nanorods) | 24:72:4 | $Fe_{25}Co_{71}/Pt_4$ | 1 | 804 | 136 |
| S5 (nanoparticles) | 16:80:4 | $Fe_{15}Co_{81}/Pt_4$ | | 560 | 119 |

This investigation has well realized the control of nanorod length, which further supplied the solution to the tunable magnetic property and dechlorination ability of hydrochloricether of as-obtained FeCo/Pt nanorods, suggesting their potential application in catalysis, environment treatment, sensors, magnetic devices, and so on.

## 2. EXPERIMENTAL PROCEDURES

**2.1. Chemicals.** All the reagents used in this work, including $H_2PtCl_6 \cdot 6H_2O$ (99%), $Fe_2(C_2O_4)_3 \cdot 5H_2O$ (99%), $Co(CH_3COO)_2 \cdot 4H_2O$ (99%), hexane ($C_6H_{14}$, 99%), ethanol ($C_2H_5OH$, 99%), propylene glycol ($C_3H_8O_2$, 99%), and 1,1,2,2-tetrachloroethane (1,1,1,2-TeCA, 99%) were purchased from Sinopharm Chemical Reagent Co., Ltd. (SCRC) and were used without further purification.

**2.2. Synthesis.** In a typical process to prepare $Fe_{40}Co_{56}/Pt_4$ nanorods, first, 2 mL of ethyl alcohol was mixed with 3 mmol of $Fe_2(C_2O_4)_3 \cdot 5H_2O$, 3 mmol of $Co(CH_3COO)_2 \cdot 4H_2O$, and 0.25 mmol of $H_2PtCl_6 \cdot 6H_2O$ at room temperature. The mixture was dissolved by ultrasonic dispersion. Four milliliters of propylene glycol was injected, and the mixture was maintained in the autoclave. The reaction system was sealed and treated at a heating rate of 2 °C · $min^{-1}$ from 30 to 180 °C and kept for 10 h. After the reaction was cooled to room temperature, the products were collected at the bottom of the container. The products were alternately washed by a hexane/ethanol mixture and deionized water with centrifugation thrice, and then they were redispersed and stored in ethanol. In addition, the other FeCo/Pt samples were prepared using the initial molar ratios of $Fe^{3+}$:$Co^{2+}$:$Pt^{4+}$ at 90:10:4(S0), 80:16:4 (S1), 72:24:4 (S2), 48:48:4 (S3), 24:72:4 (S4), and 16:80:4 (S5), for the composition of $Fe_{82}Co_{14}/Pt_4$, $Fe_{77}Co_{19}/Pt_4$, $Fe_{69}Co_{24}/Pt_4$, $Fe_{40}Co_{56}/Pt_4$, $Fe_{25}Co_{71}/Pt_4$, and $Fe_{15}Co_{81}/Pt_4$, respectively. S3a and S3b were obtained by the keeping time of 15, 30, 180, and 300 min at 180 °C, respectively. The nanoparticles were obtained by keeping them at 180 °C directly.

**2.3. Atomic Absorption Spectrometer (AAS) Measurement Experiments.** Two milliliters of aqua regia was added to the vial to digest the serials of dried FeCo/Pt nanoalloys of 1.25 mg. The resulting solution was heated to ~50 °C for 3 h. The solution changed color from a light yellow to a bright neon green. After 3 h of digestion, the solution was allowed to cool down and was diluted by deionized water to the appropriate concentration for the atomic absorption experiment. The measurement results show that the FeCo/Pt nanoalloys contain (by molar %) 82% of Fe, 14% of Co, and 4% of Pt for S0; 77% of Fe, 19% of Co, and 4% of Pt for S1; 69% of Fe, 27% of Co, and 4% of Pt for S2; 40% of Fe, 56% of Co, and 4% of Pt for S3; 25% of Fe, 71% of Co, and 4% of Pt for S4; and 15% of Fe, 81% of Co, and 4% of Pt for S5. Molar ratios of metal ions in the initial solution and the as-obtained components of FeCo/Pt nanoalloys are listed in Table 1.

**2.4. Reactivity Experiments.** All reactivity tests were carried out in vials (10 mL, nominal volume) that were tightly sealed using a Teflon-faced cover and laboratory film. As-prepared FeCo/Pt nanorods were weighed into vials that were then filled with a deoxygenated buffer solution. Each vial contained 0.1 M NaCl/25 mM Tris buffer (~pH 7.0) and an FeCo/Pt nanorod loading of 2.0 g/L. Then 160 $\mu$L of a solution of 55.56 mM 1,1,2,2-tetrachloroethane (1,1,2,2-TeCA) in hexane was added to the sealed vial via a 100 $\mu$L syringe, resulting in a final concentration of 150 $\mu$g/mL(~889 $\mu$M). A solution sample free of any FeCo/Pt nanorods was also performed and used to determine the initial concentration of 1,1,2,2-TeCA in the reactors. The vials were mixed on a rotary shaker (Shanghai Jinghong, Model TQZ-312) at 50 rpm and an ultrasonic instrument at room temperature. The presence of $Fe^{2+}$ was analyzed by AAS in the dechlorination process of 1,1,2,2-TeCA by FeCo/Pt nanorods. At each sampling time, 100 $\mu$L was removed from the reactor by simultaneously adding an equivalent volume of buffer in order to prevent the development of headspace over time. Then, the sample solution was extracted using 1.5 mL of hexane followed by subsequent dilutions with hexane and preserved at low temperature after being sealed properly. The diluted extracts were analyzed via a 5973N-6890N Gas Chromatograph−Mass Spectrum (GC-MS) (Agilent Tech.) and gas chromatograph (Thermo Finnigan Trace GC Ultra) with electron capture detection (ECD) and an RTX-1 column (DB-5MS, 30 m × 0.25 mm × 0.25 $\mu$m film thickness). Standards for analyses (1,1,2,2-TeCA and dichloroethylene (DCE)) were also performed under the same conditions.

**2.5. Characterization.** Scanning electron microscope (SEM) images were obtained with a Philip XL30 (Holland) scanning electron microscope. Transmission electron microscopy (TEM) and high resolution TEM images were taken on a JEOL JEM-1200EX microscope (Japan). Scanning transmission electron microscopy (STEM) and elemental maps were carried out under the bright field (BF) mode on a JEOL JEM-2100 F microscope. Energy dispersive X-ray (EDX) analysis of nanoalloys was conducted at 20 keV on a TN5400 EDS instrument (oxiford). Powder element analysis of Fe, Co, and Pt was measured at $\lambda$ = 248.3, 240.7, and 265.9 nm by a graphite furnace atomic absorption spectrometer (AAS) (6810, Shanghai Chromatogram Technology Company, China). X-ray diffraction analysis (XRD) was recorded using a Bruker D8 (German) diffractometer with a Cu K$\alpha$ X-ray radiation source ($\lambda$ = 0.154056 nm). X-ray photoelectron spectroscopy (XPS) experiments were carried out on an RBD upgraded PHI-5000C ESCA system (Perkin-Elmer) with Mg K$\alpha$ radiation ($h\nu$ = 1253.6 eV) or Al K$\alpha$ radiation ($h\nu$ = 1486.6 eV). Binding energies were calibrated by using the containment carbon (C1s = 284.6 eV). Vibration sample magnetometry (VSM) was used to examine the magnetic properties of FePt nanoparticles on a lakeshore7312 instrument; data are summarized in Table 1. The analysis of the degradation products was performed on a 5973N-6890N GC-MS (Agilent Tech.) and gas chromatograph (Thermo Finnigan Trace GC Ultra) with electron capture detection (ECD) and an RTX-1 column (DB-5MS, 30 m × 0.25 mm × 0.25 $\mu$m).

## 3. RESULTS AND DISCUSSION

**3.1. Characterization of FeCo/Pt Nanorods.** Figure 1 illustrates FeCo/Pt nanorods with controllable length. The SEM images show the $Fe_{40}Co_{56}/Pt_4$ nanorods with a diameter of ~80 nm and a length of ~1.7 $\mu$m (Figure 1A). In Figure 1B, it can be clearly observed in the TEM image that each FeCo rod is growing on one Pt tip (~80 nm) to form a FeCo/Pt nanorod in which each nanotip is composed of Pt nanoparticles with an average diameter of ~8 nm. In the top inset of Figure 1B, a selected-area electron diffraction pattern (SADP) recorded from a single FeCo nanorod shows the single crystal diffraction pattern


dx.doi.org/10.1021/ic201410f |Inorg. Chem. 2011, 50, 9393–9399

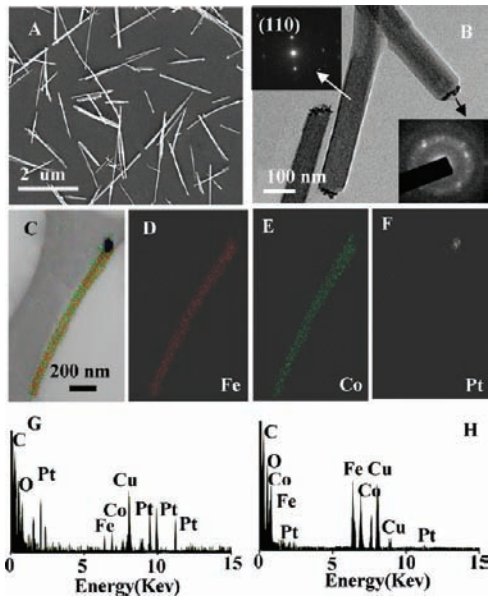


**Figure 1.** (A) SEM image of FeCo/Pt nanorods (1.7 $\mu$m × 80 nm); (B) TEM image of FeCo nanorods on Pt nanotips (80 nm) with insets of SADP images recorded from a single FeCo nanorod and Pt nanotip shown above and below; (C) BF-STEM image; (D−F) elemental maps for Fe, Co, and Pt of a single FeCo/Pt nanorod; (G,H) EDX recorded from one Pt nanotip with an inset of an HRTEM image and a single FeCo nanorod.

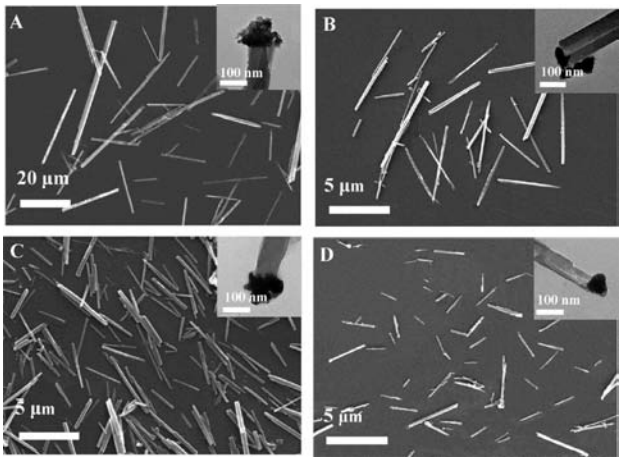


**Figure 2.** SEM images with inset TEM images of FeCo/Pt heterostructure nanorods within different Pt content: (A) FeCo/$Pt_2$ nanorods (4.5 $\mu$m). (B) FeCo/$Pt_4$ nanorods (1.7 $\mu$m). (C) FeCo/$Pt_6$ nanorods (1.0 $\mu$m). (D) FeCo/$Pt_8$ nanorods (0.6 $\mu$m).

with the indexed plane of (110). The SADP recorded from a Pt nanotip, shown in the Figure 1B inset below, illustrates the crystalline spot ring corresponding to the polycrystalline structure. The elemental distributions of the FeCo/Pt nanorods were studied by bright field scanning TEM (BF-STEM). Figure 1C shows a representative STEM image. Figure 1D−F illustrates the corresponding EDX maps for Fe, Co, and Pt in an FeCo/Pt nanorod, confirming the nanostructure of an FeCo nanorod based on a Pt nanotip. Selected area EDX analysis performed on both a single alloy rod and a metallic tip undoubtedly indicates

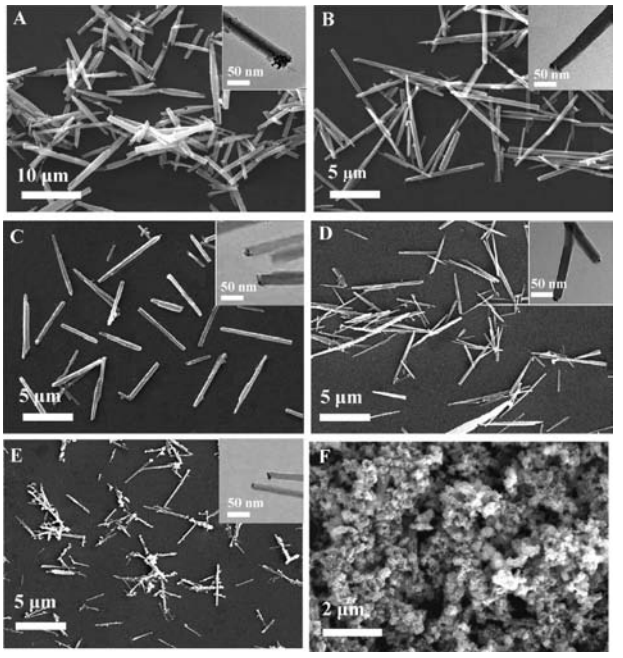


**Figure 3.** SEM images with inset TEM images of FeCo/Pt nanoalloys: (A) $Fe_{82}Co_{14}/Pt_4$ nanorods (~4 $\mu$m). (B) $Fe_{77}Co_{19}/Pt_4$ nanorods (~2.5 $\mu$m). (C) $Fe_{69}Co_{27}/Pt_4$ nanorods (~2 $\mu$m). (D) $Fe_{40}Co_{56}/Pt_4$ nanorods (~1.7 $\mu$m). (E) $Fe_{25}Co_{71}/Pt_4$ nanorods (~1 $\mu$m). (F) $Fe_{15}Co_{81}/Pt_4$ nanoparticles (~50 nm).

that the tip contains Pt (Figure 1G), and the stick is an FeCo alloy with the ratio of ~1/1 (Figure 1H). The composition analysis data by atomic absorption spectroscopy (AAS) and EDX for the other FeCo/Pt nanoalloys are given in Table 1. In addition, the precursor concentration of $Pt^{4+}$ can influnce the length of FeCo/Pt nanorods. As shown in Figure 2, the SEM images with inset TEM images show that the concentration of $Pt^{4+}$ in the initial reaction solution system at 2, 4, 6, and 8% gave nanorods with the lengths of ~4.5, 1.7, 1, and 0.6 $\mu$m, respectively. Therefore, for the given concentration of $Fe^{3+}$ and $Co^{2+}$ in the reaction system, shorter FeCo nanorods can be obtained by more Pt nanotips in a higher concentration of $Pt^{4+}$ and longer FeCo nanorods can be constructed by less Pt nanotips in a lower concentration of $Pt^{4+}$ since the number of Pt active catalysis tips depends on the precursor concentration of $Pt^{4+}$ in the initial reaction solution. The SEM images with inset TEM images of other FeCo/Pt nanoalloys are presented in Figure 3. For a given Pt content of 4%, with the decrease of Fe content in $Fe_xCo_{96-x}/Pt_4$ from 77 to 15, the morphology changes from nanorods to nanoparticles in $Fe_{15}Co_{81}/Pt_4$. The length of the nanorods are ~4, 2.5, 2, 1.7, and 1 $\mu$m for $Fe_{82}Co_{14}/Pt_4$, $Fe_{77}Co_{19}/Pt_4$, $Fe_{69}Co_{27}/Pt_4$, $Fe_{40}Co_{56}/Pt_4$, and $Fe_{25}Co_{71}/Pt_4$, respectively. Thus, the considerable length of the FeCo rods is strongly relative to the component ratio between Fe and Co. The length of a nanorod decreases with the decrease of Fe content while the Co content increases.

Their structures were also characterized by XRD. The typical XRD pattern is shown in Figure 4 for the series of FeCo/Pt nanoalloys. They all agree well with the bulk FeCo crystal structure[13] and face-centered cubic Pt.[14] A slight broadened peak can be explained by the incomplete crystallization of a small amount of amorphous alloy and nanoscale size as-obtained FeCo/Pt product. The valence of Fe, Co, and


dx.doi.org/10.1021/ic201410f |*Inorg. Chem.* 2011, 50, 9393–9399

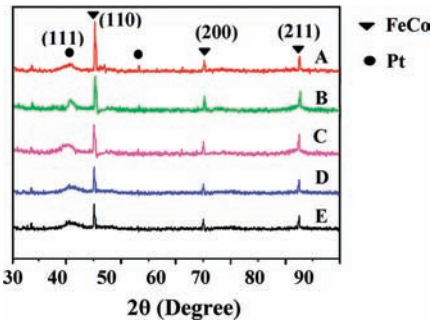


**Figure 4.** XRD of FeCo/Pt nanoalloys in different compositions: (A) $Fe_{77}Co_{19}/Pt_4$, (B) $Fe_{69}Co_{27}/Pt_4$, (C) $Fe_{40}Co_{56}/Pt_4$, (D) $Fe_{25}Co_{71}/Pt_4$, and (E) $Fe_{15}Co_{81}/Pt_4$.

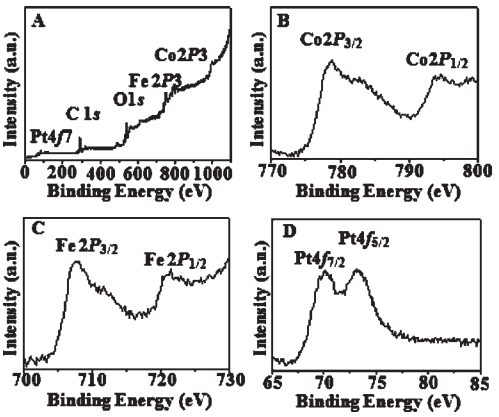


**Figure 5.** (A) XPS spectra for FeCo/Pt nanorods and (B–D) detailed spectra of Co2p, Fe2p, and Pt4f, respectively. All horizontal axes represent the binding energy corrected by that of C1s.

Pt were also investigated through XPS measurements. XPS of the $Fe_{40}Co_{56}/Pt_4$ nanorods show five photoemission peaks for Co2p, Fe2p, C1s, O1s, and Pt4f in Figure 5A. Magnified Co2p peaks, consisting of two peaks, 778.9 and 794.5 eV, are due to the spin–orbit splitting of $2p_{3/2}$ and $2p_{1/2}$ (Figure 5B), indicating that Co(0) is dominant on the surface of FeCo/Pt nanorods.[15] For Fe 2p, two peaks in Figure 5C resulting from the 2p electrons multiplet-splitting are $2p_{3/2}$ and $2p_{1/2}$ with the binding energy (BE) values of 707.7 and 720.1 eV, respectively, for Fe(III) and Fe(0).[16] In Figure 5D, two Pt4f peaks of 70.3 and 73.6 eV owing to the spin–orbit doublet splitting of $4f_{7/2}$ and $4f_{5/2}$, correspond to Pt(0).[16] On the other hand, the O1s peak of 528.7 eV implies that the oxygen ($O^{2-}$) species[16] existed on the surface of the nanoparticles and confirmed the oxide species of iron.

The length-controllable catlyzing-synthesis process of FeCo/Pt nanorods was performed through the reduction of $Fe_2(C_2O_4)_3 \cdot 5H_2O$, $Co(CH_3COO)_2 \cdot 6H_2O$, and $H_2PtCl_6 \cdot 6H_2O$ by propylene glycol in a template-absent chemical reaction system via a slow heating treatment. It can be suggested that the construction of an FeCo/Pt nanorod can be driven by the catalysis of Pt nanotips and the anisotropic cubic crystalline structure of FeCo. The length-controllable preparation of FeCo nanorods based on the Pt nanotips is shown in Scheme 1. In the present template-absent reaction system, $Pt^{4+}$ was first reduced by propylene glycol and aggregated into nuclear active nanotips

**Scheme 1. Scheme of the Formation Of FeCo/Pt Nanorods**[a]

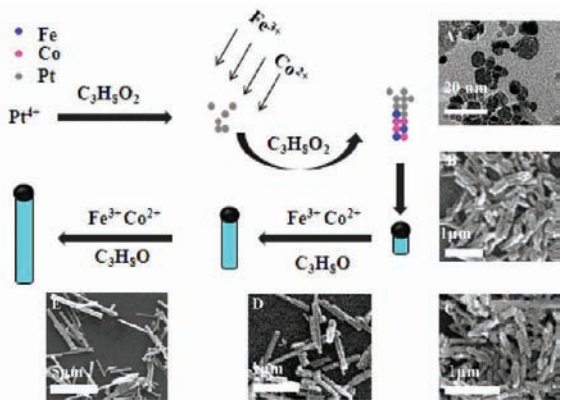


[a] Inset TEM and SEM images obtained at different growth periods: (A) stop at 130 °C for 0 min (TEM image). (B–E) Maintain the stop temperature at 180 °C for 15, 30, 180, and 600 min.

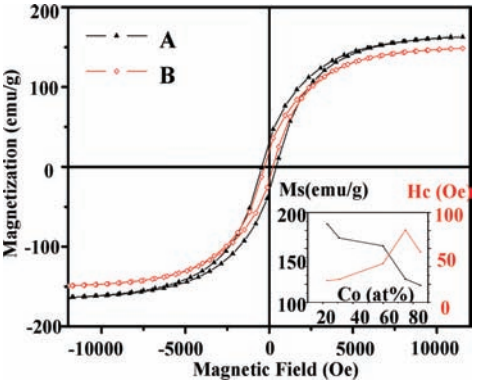


**Figure 6.** Room-temperature length-dependent hysteresis loops of $Fe_{40}Co_{56}/Pt_4$ nanoalloys with different shapes: (A) nanorods and (B) nanoparticles. The inset shows that the length-dependent variation of magnetization and coercivity resulted by the different molar ratios of Fe/Co in FeCo/Pt nanoalloys.

during the early stage of the reaction. Main products of Pt nanoparticles with a diameter of ~8 nm could be observed in the TEM image A of Scheme 1 by stopping the reaction at the early synthesis stage at 130 °C. Then, on the basis of the catalysis of Pt nanotips, $Fe^{3+}$ and $Co^{2+}$ were reduced and alloyed. Because the anisotropic fcc crystalline structure of the FeCo allows for the selective growth on a different crystal plane, the induced growth thus leads to a preferential growth along the axis of the FeCo nanorods deposited on Pt nanotips. The length of the FeCo nanorods increased as the time continued. In addition, FeCo nanorods make growth more favorable on the Fe rich facets and lead to the long nanorods in high Fe concentration samples (Figure 3). The growth process of FeCo/Pt nanorods were monitored by TEM and SEM measurements via maintaining the stopping temperature at 130 °C for 0 min and at 180 °C for 15, 30, 180, and 600 min. In the insets of Scheme 1, the TEM and SEM images of FeCo/Pt obtained during different reaction stages confirm the mechanism analysis of the above formation process.

**3.2. Magnetic Properties of FeCo/Pt Nanoalloys.** The magnetic hysteresis measurement results indicate that the


dx.doi.org/10.1021/ic201410f |*Inorg. Chem.* 2011, 50, 9393–9399

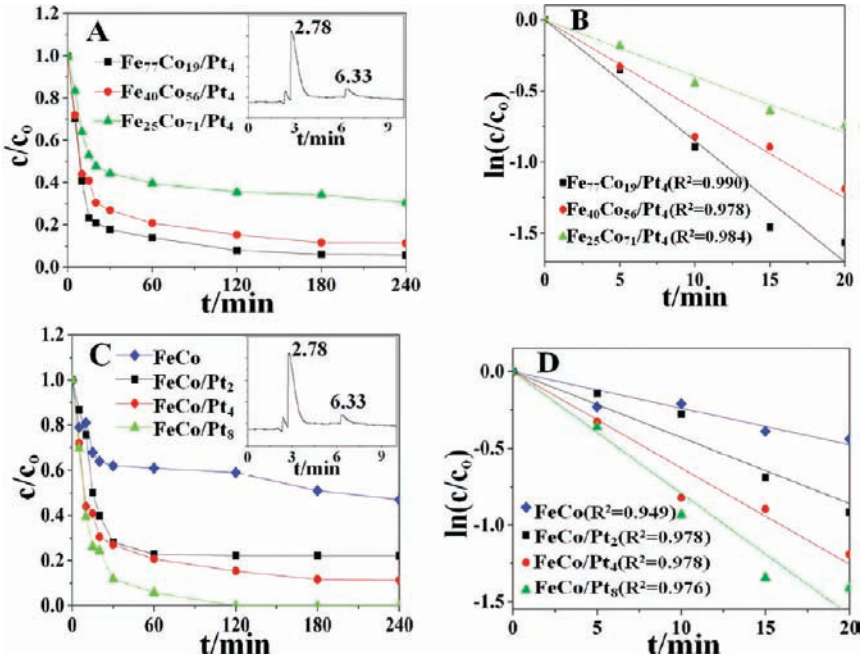


**Figure 7.** (A,C) Variations of 1,1,2,2-TeCA concentration over time under degradation of $Fe_xCo_{96-x}/Pt_4$ and $FeCo/Pt_x$ nanorods with an inset of the GC spectrum of the degradation sample solution at 60 min. The peaks at $t = 2.78$ and $t = 6.33$ min correspond to DCE and 1,1,2,2-TeCA, respectively. (B,D) Plots of pseudofirst-order reaction regressions of $Fe_xCo_{96-x}/Pt_4$ and $FeCo/Pt_x$ nanorods.

magnetic property is dependent on both the shape and the length of the FeCo/Pt nanorods, which resulted from the composition. In Figure 6, the saturation magnetizations ($M_s$) of 195.9 and 162.7 emu/g with the coercivity ($H_c$) of 410.0 and 430.3 Oe are given for $Fe_{40}Co_{56}/Pt_4$ nanoparticles and nanorods, respectively. In the inset of Figure 6, two broken line graphs show $M_s$ and $H_c$ versus the Fe/Co molar ratio of the FeCo/Pt nanoalloys. The values of $M_s$ are 187, 172, 163, 136, and 119 emu/g for $Fe_{77}Co_{19}/Pt_4$ (~2.5 $\mu$m), $Fe_{69}Co_{27}/Pt_4$ (~2 $\mu$m), $Fe_{40}Co_{56}/Pt_4$ (~1.7 $\mu$m), $Fe_{25}Co_{71}/Pt_4$ (~1 $\mu$m), and $Fe_{15}Co_{81}/Pt_4$ (~0.05 $\mu$m), respectively, and their corresponding values of $H_c$ are 240, 256, 430, 804, and 560 Oe. $Fe_{77}Co_{19}/Pt_4$, with an average length of ~2.5 $\mu$m being the best soft magnetic property with the largest maximum saturation magnetization of 187 emu/g and the lowest minimum coercivity of 240 Oe, which is consistent with that for the bulk FeCo alloy.[17] Thus, the increase of the nanorod length, as a result of the molar ratio of Fe/Co, leads to the decrease of $M_s$ and increase of $H_c$. The detailed quantitative magnetic data are summarized in Table 1.

**3.3. Reactivity of FeCo/Pt nanorods.** Because zerovalent iron is an effective reductant toward a broad spectrum of pollutants including chlorinated solvents, and metallic Fe is known to be the primary source of reducing equivalents in a bimetallic alloy system,[18] the series of experiments were performed to investigate the reactivity of the as-synthesized FeCo/Pt nanorods toward a model organohalid and thus could have potential applications in environmental remediation. In addition, bimetallic zerovalent irons, like Fe/Ni and Fe/Pd, are more reactive toward organohalides relative to the zerovalent iron.[19] It is proposed that bimetallic reductants are more reactive than metallic iron as a result of the additives (e.g., Ni and Pd) having superior ability to sorb atomic hydrogen generated via the reduction of water, and this atomic hydrogen is postulated to be the reactive entity responsible for degrading chlorinated hydrocarbons through a surface-mediated reaction. Hence, three samples of FeCo/Pt nanorods with different lengths, $Fe_{77}Co_{19}/Pt_4$ (~2.5 $\mu$m), $Fe_{40}Co_{56}/Pt_4$ (~1.7 $\mu$m), and $Fe_{25}Co_{71}/Pt_4$ (~1 $\mu$m), were selected by assuming that they also have the largest amount of reducing equivalents. These FeCo/Pt nanorods exhibit length-dependent reactivity toward the reductive dechlorination of 1,1,2,2-tetrachloroethane (1,1,2,2-TeCA) with a symmetrical structure. Figure 7 illustrates the variations in 1,1,2,2-TeCA concentration over time in reactivity experimental systems with each of the above selected $Fe_xCo_{96-x}/Pt_4$ nanorods, which were examined by a gas chromatograph−mass spectrum (GC-MS). In Figure 7A, almost 95% degradation of the 1,1,2,2-TeCA was observed in $Fe_{77}Co_{19}/Pt_4$ with the length of ~2.5 $\mu$m over a 120 min reaction. In contrast, $Fe_{40}Co_{56}/Pt_4$ and $Fe_{25}Co_{71}/Pt_4$ with the lengths of ~1.7 $\mu$m and ~1 $\mu$m reduced 80% and 60% of the initial 1,1,2,2-TeCA over 120 min, respectively, with no further loss being observed over the remainder of the experiment. In particular, high Pt content samples are more reactive toward 1,1,2,2-TeCA than that of lower Pt content (Figure 7C). $FeCo/Pt_8$ shows almost a complete degradation of 1,1,2,2-TeCA over a 120 min reaction. In contrast, it can be observed that $FeCo/Pt_4$ reduced 85% and $FeCo/Pt_2$ reduced 75% of the initial 1,1,2,2-TeCA over 120 min, and further loss is not observed over the remainder of the experiment. Furthermore, if Pt is absent, FeCo nanoalloys only reduce 50% of the initial 1,1,2,2-TeCA over 180 min. Therefore, Pt could enhance the dechlorination activity. As seen in an electron capture detector (ECD) GC spectra (inset of Figure 7A,C), two kinds of dechlorination products of DCE were detected for all of the $Fe_xCo_{96-x}/Pt_4$ nanorods, which were examined in the degradation sample solution at 60 min in this investigation. It confirms that our as-synthesized FeCo/Pt nanorods are effective for the dechlorination of 1,1,2,2-TeCA and that Pt enhances the reactivity of dechlorination. This is


dx.doi.org/10.1021/ic201410f |*Inorg. Chem.* 2011, 50, 9393–9399

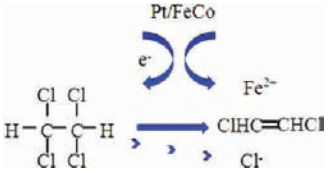


**Figure 8.** Mechanism scheme of the degradation process by FeCo/Pt nanorods on 1,1,2,2-TeCA.

consistent with previous studies that have also reported reductive $\beta$-elimination as the dominant transformation pathway for 1,1,2,2-TeCA in zerovalent metal systems.[20]

The dechlorination process of FeCo/Pt nanoalloys toward 1,1,2,2-TeCA is suggested in Figure 8. As it is well known, there are two steps in the reduction decholorination of hydrochloricether by Fe(0) in aqueous solution. First, hydrochloricether is absorbed on the iron surface and catches the electrons released from iron, then reduction decholorination occurs via the following reaction:

$$Fe + H^+ + RCl_x \rightarrow Fe^{2+} + RHCl_{x-1} + Cl^-$$

Second, a certain amount of new fresh H· with a strong reducibility will be generated during the corrosion of iron, and the H· can indirectly reduce hydrochloricether by the following reactions:

$$Fe + H_2O \rightarrow Fe(OH)_2 + 2H\cdot$$

$$H\cdot + RCl_x + e^- \rightarrow RHCl_{x-1} + Cl^-$$

In multimetallic reductants of FeCo/Pt, Fe(0) acts as the reducing agent to supply electrons to 1,1,2,2-TeCA. The coupling of a less reactive noble metal, Pt, to a more reactive metal, Fe, can accelerate the oxidation of the more reactive metal; thus, Pt can distinctly enhance the reactivity. The detailed explanation is as follows: first, the degradation process is generally accepted to be electrochemical in nature, including a simple dechlorination process, with Fe(0) serving as the source of electrons, where oxidation of the iron and reduction chlorination of 1,1,2,2-TeCA take place. The presence of $Fe^{2+}$ was analyzed by an AAS measurement during the dechlorination process of 1,1,2,2-TeCA by FeCo nanoalloys and FeCo/Pt nanorods. In contrast, we did blank experiments where only the 1,1,2,2-TeCA solution was analyzed. After the reaction was carried out for 30 min, the concentrations of $Fe^{2+}$ were 0, 0.042, and 0.305 ppm for the blank sample, FeCo nanoalloy, and FeCo/Pt nanorod, respectively, confirming the exsitence of $Fe^{2+}$ in this dechloration system according to the above dechlorination mechanism. In addition, the electrocatalysis in the multimetallic FeCo/Pt system can accelerate the corrosion of Fe.[21] Second, when Co alloys with Fe, the FeCo alloy can prevent iron from forming an oxide and passive film on the surface, and the effective reduction area of iron can be increased, which is benificial for the absorption of 1,1,2,2-TeCA.[22] After many iron dot corrosion areas form by the cell in the FeCo/Pt system, Fe supplies more fresh surface for the decholorination of 1,1,2,2-TeCA. Moreover, as the conductor, electrons can tranfer to the organic compound through Pt to be reduced. Third, in the reduction process of hydrochloricether, new generated H· with strong reducibility increases the reducing odds of 1,1,2,2-TeCA. Since the noble metal of Pt possesses the low hydrogen overpotential, it can easily lead to the hydrogen evolution reaction, which is benificial to the generation of more H·. Thus, the reduction decholorination speed of 1,1,2,2- TeCA is improved by the increased reaction pathway of the reduction decholorination.

Generally, the rate of pollutant transformation in zerovalent iron systems is pseudofirst-order[23,24] with respect to the pollutant concentration as shown in the following equation:

$$-d[C]/dt = k_{SA}\alpha_s\rho_m[C] = k_{obs}[C]$$

Applying this equation to the system considered here, [C] is the concentration of 1,1,2,2-TeCA ($mg\cdot L^{-1}$), $k_{SA}$ is the surface-area-normalized rate constant ($L\cdot h^{-1}\cdot m^{-2}$), $\alpha_s$ is the specific surface area of $Fe_xCo_{96-x}$ ($m^2\cdot g^{-1}$), $\rho_m$ is the mass concentration ($g\cdot L^{-1}$), and $k_{obs}$ is the observed pseudofirst-order rate constant (per h). As shown in Figure 7B, the concentration of 1,1,2,2-TeCA initially followed an exponential decay in each reactor system, although deviations from this model consistent with surface passivation were observed for $Fe_{40}Co_{56}/Pt_4$ and $Fe_{25}Co_{71}/Pt_4$ nanorods at greater time scales. Linear regression analysis performed over the time period shown in Figure 7B was therefore used to determine the initial $k_{obs}$ value for the 1,1,2,2-TeCA reduction by $Fe_{77}Co_{19}/Pt_4$ (~2.5 $\mu$m), $Fe_{40}Co_{56}/Pt_4$ (~1.7 $\mu$m), and $Fe_{25}Co_{71}/Pt_4$ (~1 $\mu$m). These values were determined to be 4.69, 3.57, and 2.22 $h^{-1}$, respectively. The FeCo/Pt nanorods presented length-dependent reactivity, and the longer length gives the more reactive dechlorination. In this work, $k_{obs}$ of $Fe_{77}Co_{19}/Pt_4$ (~2.5 $\mu$m) demonstrates roughly a 2-fold greater reactivity relative to $Fe_{25}Co_{71}/Pt_4$ (~1 $\mu$m). In addition, linear regression analysis performed over the time period shown in Figure 7D was also used to determine the initial $k_{obs}$ value for the 1,1,2,2-TeCA reduction by FeCo, $FeCo/Pt_2$, $FeCo/Pt_4$, and $FeCo/Pt_8$. These values were determined to be 1.32, 2.75, 3.57, and 4.23 $h^{-1}$, respectively, indicating that Pt content influnces the reactivity of the dechlorination of 1,1,2,2-TeCA by FeCo/Pt nanorods in which the $k_{obs}$ of $FeCo/Pt_8$ proves a roughly 2- and 3-fold greater reactivity relative to that of $FeCo/Pt_2$ and FeCo, respectively.

## 4. CONCLUSION

In conclusion, a newly designed FeCo/Pt nanorod has been first reported and successfully fabricated through a length-controllable catalyzing-synthesis process. The as-obtained FeCo/Pt nanorods possess the length-controllable properties of the magnetism and catalytic activity toward the dechlorination of hydrochloricether. $Fe_{77}Co_{19}/Pt_4$ nanorods with the length of ~2.5 $\mu$m have the best soft magnetic property with the maximum saturation magnetization and minimum coercivity. They also yield the greatest reductive rate of dechlorination of 1,1,2,2-tetrachloroethane, where especially Pt nanotips can enhance the dechlorination activity. Therefore, the as-obtained FeCo/Pt nanorods, with the combination function in magnetics and the dechlorination of hydrochloricether by FeCo nanorods as well as the enhancement dechlorination by Pt nanotips, can be ideal building blocks for the active sites included in high-performance magnetic devices. This investigation provided a good way to grow one-dimensional alloy nanomaterials and will be of great significance for the applications in magnetics, industry catalysis, environment treatment, biomedical, sensors, and other devices.

## AUTHOR INFORMATION

### Corresponding Authors

*Phone: +86-21-65982653 ext. 8544. Fax: +86-21-65981097. Email: m_wen@tongji.edu.cn (M.W.), qswu@tongji.edu.cn (Q.W.).

## ACKNOWLEDGMENT

This work was financially supported by the National Natural Science Foundation of China (21171130 and 51072134), the State Major Research Plan (973) of China (2011CB932404), the Key Program for the Basic Research of SSTCF (09JC1414100), and the Innovation Program of SECF (10ZZ21) from China.

## REFERENCES

(1) Hu, X. L.; Yu, J. C. *Chem. Mater.* **2008**, *20*, 6743–6749.

(2) (a) Burkert, T.; Nordstrom, L.; Eriksson, O.; Heinonen, O. *Phys. Rev. Lett.* **2004**, *93*, 027203. (b) Winkelmann, A.; Przybylski, M.; Luo, F.; Shi, Y.; Barthel, J. *Phys. Rev. Lett.* **2006**, *96*, 257205. (c) Yildiz, F.; Luo, F.; Tieg, C.; Abrudan, R. M.; Fu, X. L.; Winkelmann, A.; Przybylski, M.; Kirschner, J. *Phys. Rev. Lett.* **2008**, *100*, 037205.

(3) (a) Sun, S.; Murray, C. B.; Weller, D.; Folks, L.; Moser, A. *Science* **2000**, *287*, 1989–1992. (b) Antoniak, C.; Lindner, C. J.; Spasova, M.; Sudfeld, D.; Acet, M.; Farle, M. *Phys. Rev. Lett.* **2006**, *97*, 117201.

(4) (a) Wei, X. W.; Zhu, G. X.; Liu, Y. J.; Ni, Y. H.; Song, Y.; Xu, Z. *Chem. Mater.* **2008**, *20*, 6248–6253. (b) Nguyen, Q.; Chinnasamy, N.; Yoon, S. D.; Sivasubramanian, S.; Skai, T.; Baraskar, A.; Mukerjee, S.; Vittoria, C.; Harris, V. G. *J. Appl. Phys.* **2008**, *103*, 07D532.

(5) (a) Zeng, H.; Li, J.; Liu, J. P.; Wang, Z. L.; Sun, S. *Nature* **2002**, *420*, 395–398. (b) Zeng, H.; Li, J.; Wang, Z. L.; Liu, J. P.; Sun, S. *Nano Lett.* **2004**, *4*, 187–190. (c) Behrens, S.; Bonnemann, H.; Matoussevitch, N.; Gorschinski, A.; Dinjus, E.; Habicht, W.; Bolle, J.; Zinoveva, S.; Palina, N.; Hormes, J.; Modrow, H.; Bahr, S.; Kempter, V. *J. Phys.: Condens. Matter.* **2006**, *18*, 2543–2561.

(6) (a) Bai, J.; Wang, J. P. *Appl. Phys. Lett.* **2005**, *87*, 152502–152505. (b) Sharif, R.; Shamaila, S.; Ma, M.; Yao, L. D.; Yu, R. C.; Han, X. F.; Wang, Y.; Khaleequr- Rahman, M. *J. Magn. Magn. Mater.* **2008**, *320*, 1512–1516.

(7) (a) Khan, H. R.; Petrikowski, K. *Mater. Sci. Eng., C* **2002**, *19*, 345–348. (b) Li, F. S.; Zhou, D.; Wang, T.; Wang, Y.; Song, L. J.; Xu, C. T. *J. Appl. Phys.* **2007**, *101*, 014309.

(8) (a) Sun, S. *Adv. Mater.* **2006**, *18*, 393–403. (b) Tzitzios, V.; Niarchos, D.; Gjoka, M.; Boukos, N.; Petridis, D. *J. Am. Chem. Soc.* **2005**, *127*, 13756–13757.

(9) (a) Wen, M.; Zhu, Y. Z.; Wu, Q. S.; Zhang, F.; Zhang, T. *J. Phys. Chem. C* **2009**, *113*, 5960–5966. (b) Wen, M.; Yang, D.; Wu, Q. S.; Lu, R. P.; Zhu, Y. Z.; Zhang, F. *Chem. Commun.* **2010**, *46*, 219–221.

(10) (a) Wang, D. S.; Li, Y. D. *J. Am. Chem. Soc.* **2010**, *132*, 6280–6281. (b) Habas, S. E.; Lee, H.; Radmilovic, V.; Somorjai, G. A.; Yang, P. *Nat. Mater.* **2007**, *6*, 692–697.

(11) Zhang, F.; Wen, M.; Cheng, M. Z.; Liu, D.; Zhu, A. W.; Tian, Y. *Chem. Eur. J.* **2010**, *16*, 11115–11120.

(12) Shevchenko, E. V.; Talapin, D. V.; Rogach, A. L.; Kornowski, A.; Haase, M.; Weller, H. *J. Am. Chem. Soc.* **2002**, *124*, 11480–11485.

(13) Wei, X. W.; Zhu, G. X.; Liu, Y. J.; Ni, Y. H.; Song, Y.; Xu, Z. *Chem. Mater.* **2008**, *20*, 6248–6253.

(14) Liang, H. W.; Liu, S.; Gong, J. Y.; Wang, S. B.; Wang, L.; Yu, S. H. *Adv. Mater.* **2009**, *21*, 1–5.

(15) Su, X. B.; Zheng, H. G.; Yang, Z. P.; Zhu, Y. C.; Pan, A. L. *J. Mater. Sci.* **2003**, *38*, 4581–4585.

(16) Mi, W. B.; Liu, H.; Li, Z. Q.; Wu, P.; Jiang, E. Y.; Bai, H. L. *J. Appl. Phys.* **2005**, *97*, 124303.

(17) Chaubey, G. S.; Barcena, C.; Poudyal, N.; Rong, C. B.; Gao, J. M.; Sun, S. H.; Liu., J. P. *J. Am. Chem. Soc.* **2007**, *129*, 7214–7215.

(18) (a) Bokare, A. D.; Chikate, R. C.; Rode, C. V.; Paknikar, K. M. *Environ. Sci. Technol.* **2007**, *41*, 7437–7443. (b) Alowitz, M. J.; Scherer, M. M. *Environ. Sci. Technol.* **2002**, *36*, 299–306.

(19) (a) Cwiertny, D. M.; Bransfield, S. J.; Roberts, A. L. *Environ. Sci. Technol.* **2007**, *41*, 3734–3740. (b) Schrick, B.; Blough, J. L.; Jones, A. D.; Mallouk, T. E. *Chem. Mater.* **2002**, *14*, 5140–5147.

(20) (a) Hong, Y.; Rheem, Y. W.; Lai, M.; Cwiertny, D. M.; Walk, S. L.; Myung, N. V. *Chem. Eng. J.* **2009**, *151*, 66–72. (b) Song, H.; Carraway, E. R. *Environ. Sci. Technol.* **2005**, *39*, 6237–6245.

(21) O'Loughlin, E. J.; Kemner, K. M.; Burris, D. R. *Environ. Sci. Technol.* **2003**, *37*, 2905–2912.

(22) Clark, C. J.; Rao, P. S. C.; Annable, M. D. *J. Hazard. Mater.* **2003**, *B96* (1), 65–78.

(23) Lien, H. L.; Zhang, W. X. *Appl. Catal., B* **2007**, *77*, 110–116.

(24) Zhang, L.; Arnold, W. A.; Hozalski, R. M. *Environ. Sci. Technol.* **2004**, *38*, 6881–6889.